



A Thermodynamics Model for the Assessment and Optimisation of Onboard Natural Gas Reforming and Carbon Capture

Li Chin Law^{1,2} · Epaminondas Mastorakos^{1,3} · Mohd. Roslee Othman³ · Antonis Trakakis⁴

Received: 31 March 2023 / Revised: 17 July 2023 / Accepted: 18 November 2023 / Published online: 6 December 2023
© The Author(s) 2023

Abstract The paper examines pre-combustion carbon capture technology (PreCCS) for liquefied natural gas (LNG) propelled shipping from thermodynamics and energy efficiency perspectives. Various types of LNG reformers and CCS units are considered. The steam methane reformer (SMR) was found to be 20% more energy efficient than autothermal (ATR) and methane pyrolysis (MPR) reactors. Pressure swing adsorption (PSA) had a lower energy requirement than membrane separation (MEM), cryogenic separation (CS), and amine absorption (AA) in pre-combustion carbon capture, with PSA needing 0.18 kWh/kg CO₂. An integrated system combining SMR and PSA was proposed using waste heat recovery (WHR) from the engine, assuming similar efficiency for LNG and H₂ operation, and cooling and liquefying of the CO₂ by the LNG. The SMR-PSA system without WHR had an overall efficiency of 33.4% (defined as work at the propeller divided by the total LNG energy consumption). This was improved to 41.7% with WHR and gave a 65% CO₂ emission reduction. For a higher CO₂ reduction, CCS from the SMR heater could additionally be employed, giving a maximum CO₂ removal rate of 86.2% with 39% overall energy efficiency. By comparison, an amine-based post-engine CCS system without reforming could reach similar CO₂ removal rates but with 36.6% overall efficiency. The advantages and disadvantages and technology readiness level of PreCCS for onboard operation are discussed. This study offers evidence that pre-combustion CCS can be a serious contender for maritime propulsion decarbonization.

Keywords Hydrogen production · Low-carbon alternative fuel · Maritime · Methane · Ship decarbonization · Pre-combustion carbon capture

Nomenclature

AA	Amine absorption	IMO	International Maritime Organization
ACAPEX	Annualized capital cost	IMO2030	IMO decarbonization goal of 40% CO ₂ reduction by 2030
ANOVA	Analysis of variance	IMO2050	IMO decarbonization goal of 70% CO ₂ reduction by 2050
ATR	Autothermal reformer	LNG	Liquefied natural gas
CH ₄	Methane	LTWGS	Low-temperature water-gas shift
CII	Carbon intensity indicator	m _{H2}	Mass of produced hydrogen
CO	Carbon monoxide	m _{H2,out}	Mass flow of hydrogen at reactor outlet
CO ₂	Carbon dioxide	MDEA	Methyl diethanolamine
CS	Cryogenic separation	MPR	Methane pyrolysis reactor
C _T	Total production cost of hydrogen	CCS	Carbon capture and storage
EEDI	Energy efficiency design index	OCCS	Onboard carbon capture and storage
H	Enthalpy	OPEX	Operating cost
H _{feed}	Enthalpy of feed	PostCCS	Post-combustion CCS
H _{ICE,feed}	Enthalpy of feed into ICE	PreCCS	Pre-combustion carbon capture
H ₂	Hydrogen	P	Power
H ₂ O	Water	P _{ASU}	Power requirement of air separation unit
HFO	Heavy fuel oil	P _{CCS}	Power requirement for CCS
HTWGS	High-temperature water-gas shift	P _{comp}	Power requirement of methane compressor
ICE	Internal combustion engine	P _{H2O,pump}	Power requirement of water pump

Extended author information available on the last page of the article

P_{prop}	Propulsion power
PSA	Pressure swing adsorption
P_{SMR}	Pressure of SMR
Q	Heat
Q_{CCS}	Heat requirement for CCS
$Q_{\text{h,CH}_4}$	Heat produced by methane combustion in furnace
$Q_{\text{h,SMR}}$	Heat requirement for SMR
$Q_{\text{h,steam}}$	Heat requirement for steam generation
S/C	Steam to methane ratio
SMR	Steam methane reformer
TRL	Technological reliability level
T_{SMR}	Exit temperature of SMR
WGS	Water-gas shift
WHR	Waste heat recovery
WTW	Well-to-wake
X_{CH_4}	% feed of methane into furnace
$X_{\text{f,SMR}}$	% feed of methane into SMR-integrated system
ϵ_o	Energy efficiency
ϵ_r	Reactor efficiency
β_o	CO ₂ reduction efficiency
α_{H_2}	hydrogen yield

1 Introduction

Shipping decarbonization has gained increasing attention in recent years following the carbon reduction goals set by the International Maritime Organization (IMO). The adoption of low- and zero-carbon fuels for ocean-going vessels has been widely discussed for its potential to reduce carbon emissions. In 2021, IMO adopted a new target to reduce carbon emission from shipping by 40% by 2030. Zero Emission Shipping Mission was launched by Mission Innovation, with the goal to operate at least 5% of global vessels by using well-to-wake (WTW) zero-emission fuels including green hydrogen, ammonia, and biofuels by 2030 [1]. Low-carbon fuels like blue hydrogen, liquefied natural gas (LNG), and methanol also have increasing demand which could help to meet the target of carbon reductions.

Each of the alternative fuel options has different energy costs, carbon reduction potentials, financial costs, and technology readiness level, which puts stakeholders in difficulty during their decision-making process. There seems to be little investment today on these alternative options. However, the uptake of LNG as a marine fuel is advancing with an increased number of newly built LNG-fuelled ships [2]. The high technological readiness level (TRL) of LNG-fuelled vessels, with

effectiveness in reducing the energy efficiency design index (EEDI) and carbon intensity indicator (CII) of ships by 20%, makes LNG a promising transition fuel [3]. However, capturing the CO₂ produced onboard is crucial for LNG-fuelled ships to meet IMO's reduction goal. Hence, onboard carbon capture and storage (OCCS) is an attractive proposition [4]. Studies related to ship-based CCS have been carried out focusing on the techno-economic assessment of the technology to decarbonize ships. It was estimated that CCS installation consumed about 20% of the LNG fuel to operate solvent-based CCS units [5]. By comparing LNG with CCS installation with other alternative fuels like ammonia, methanol, hydrogen, and electricity, Li Chin et al. showed that the cost of CCS installation and energy requirement was lower than the other alternatives [5]. In addition to this, only post-engine CCS has been considered [4] [5], while pre-combustion CCS (i.e. reforming LNG to H₂ and capturing the CO₂) has been proposed [6] but not studied in detail yet.

Apart from LNG, the investment on the infrastructure of hydrogen is also quite notable, as evident from some ongoing large-scale projects including HySHIP [7], Topeka hydrogen project [8], and HySeas [9]. The use of hydrogen is more challenging than LNG in terms of storage due to the low energy density and extremely low boiling point (−253 °C). In terms of safety, hydrogen is less safe than LNG because the former has low minimum ignition energy, high burning velocity, and a wide flammability range [10]. In terms of cost, the cost of hydrogen per unit of propulsion energy was estimated to be three times more expensive than LNG with CCS installation due to the high hydrogen storage cost and fuel price [5] [4]. For the same propulsion energy, hydrogen needs more than 4.5 times the HFO volume; hence, for the same size of storage tank, the usage of hydrogen fuel can limit the voyage distance [5] [4]. It was also reported that the ship powered by hydrogen fuel needs to refuel three times to travel the same voyage distance as the same ship powered by HFO [4]. As highlighted by Smith et al. [11], an additional issue with liquid H₂ bunkering and storage on the ship as the propulsion fuel is its higher boil-off rate as compared to LNG, which needs a reliquefaction unit that consumes a significant amount of energy. Hence, the on-shore H₂ production and bunkering for use as a ship propulsion fuel incur significant penalties (energy and financial) and remain at low TRL at present.

Apart from the foreseeable impact with the usage of hydrogen fuel, another issue with the usage of hydrogen as a marine fuel is the bunkering infrastructure, which is still under development. The demand of hydrogen

has grown threefold since 1975 to meet the increasing demand from oil refining and ammonia manufacturing; hence, the adoption of hydrogen as marine fuel would require hydrogen production on a larger scale to meet the bunkering demand [12]. However, using mixtures of hydrogen and LNG at different compositions can reduce the economic impact, while at the same time can prepare the ship to meet the new targets of CO₂ reduction in the foreseeable future.

To resolve the above problems of hydrogen as marine fuel in terms of storage, safety, fuel availability, and low TRL bunkering infrastructure, the concept of onboard hydrogen production from LNG (see Fig. 1c, discussed later) has been introduced. Class society RINA initiated

the plan to meet 70% carbon reduction target via hydrogen production [13]. Wärtsilä in collaboration with Hycamite TCD Technologies started to develop a prototype to produce hydrogen from LNG on board via methane pyrolysis process, which gives solid carbon as the by-product [14]. The commercialized “C-Zero” unit, which is a technology for the separation of hydrogen from the carbon in the natural gas, shows that there is an increasing demand for on-site production of hydrogen fuel [15]. However, the sustainability of hydrogen fuel is closely related to the production methods and operating conditions of the processes. One of the critical questions that can be raised by shipping stakeholders is which production methods

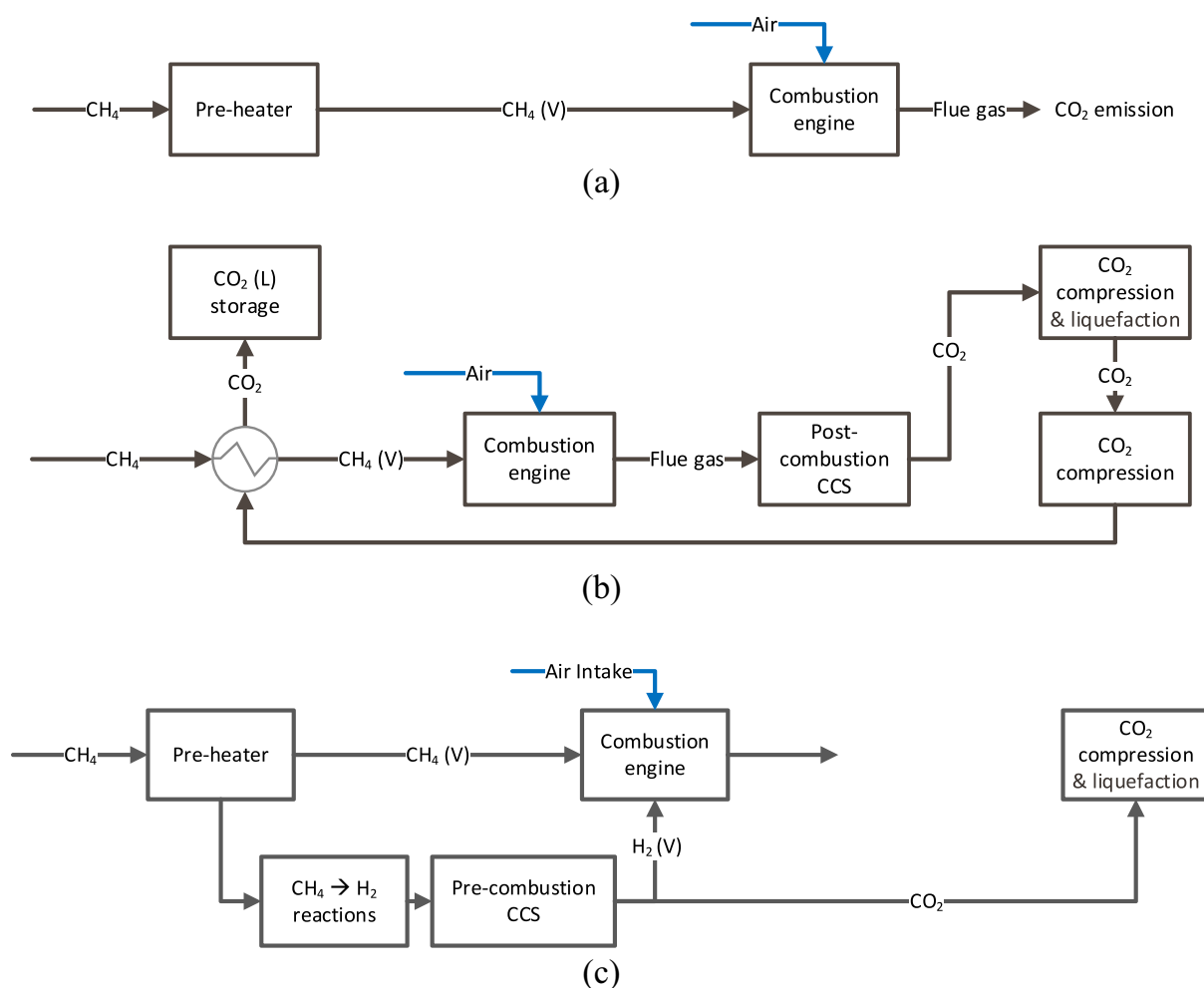


Fig. 1 Block diagram for ship powered by combustion engine with and without carbon capture. **a** Conventional ship without CCS; **b** ship integrated with post-combustion CCS, i.e. CO₂ is captured downstream of the combustion engine; **c** ship integrated with pre-combus-

tion CCS, i.e. CO₂ is captured upstream of the combustion engine which is using the reformer gas (mostly H₂) as the fuel. For configuration, various reformers and CCS units are examined in this paper.

and hydrogen separation technologies are more suitable for ship installation.

Previous studies on hydrogen production plants suggest that steam methane reforming reaction (SMR) has the highest efficiency of 70–85% [16, 17], followed by partial oxidation and autothermal reforming (ATR) which were claimed to have comparable thermal efficiency of 60–75% [16], water electrolysis (50–70%) [18], coal gasification (60%) [18], and methane pyrolysis (MPR) (58%) [17]. In terms of hydrogen purification (i.e. carbon capture), pressure swing adsorption (PSA) is one of the most common pre-combustion CCS (PreCCS) technologies. However, only about 52% CO₂ capture rate was observed for SMR if the flue gas from the reformer is not treated, allowing about 8.2 kg CO₂ emitted per kg of produced hydrogen [19] (SMR needs heat which is produced by burning methane). However, an 85% capture rate can be achieved if the reformer flue gas undergoes the post-combustion CCS [19]. In doing so, an additional 8.2% NG will be consumed [19]. Ethane pyrolysis and water electrolysis also have a considerably high carbon footprint of 4.5 kg CO₂ and 17 kg CO₂ respectively per kg of hydrogen produced [18]. Hence, the selection of hydrogen production methods and types of carbon capture can affect the overall efficiency of hydrogen production and the overall carbon footprint of a ship. This study aims to analyse a ship-based hydrogen production unit by integrating with a suitable type of pre-combustion CCS so that a desired carbon emission rate can be achieved at lower cost and energy consumption. The energy requirements of three methods of hydrogen production and four types of carbon capture units are quantified and compared so that a final proposal of a hydrogen production system for ships can be presented. Since the H₂ production, the CO₂ capture, and the H₂ combustion are taking place on the same vessel, opportunities for heat integrations emerge that can reduce the overall cost of the energy-intensive H₂ production and CO₂ capture processes. An LNG ship carries cold fuel which can also be used to help cool and liquefy the CO₂ for liquid CO₂ storage. These potentials are explored in this paper so that the possibility of an onboard PreCCS system can be fully assessed.

The feasibility to use the exhaust heat for endothermic reforming has been reported [20–24]. As justified in Ref. [25], high-temperature exhaust gas from the engine can be considered a high-grade heat source which can reduce onboard fuel consumption by about 10%. Pashchenko et al. emphasized the concept of thermochemical exhaust heat recuperation for SMR and steam generation which can improve the overall efficiency by 4–7% [20, 23]. The heat from the SMR furnace and exhaust gas was shown feasible

to pre-heat the natural gas to 773 K prior to entering the reformer; besides, the MDEA-based pre-combustion CCS was claimed to operate with almost no extra cost by utilizing the low-grade heat downstream the WGS reactors [22]. In another way of waste heat utilization, previous researchers [21, 24, 26] studied the performance of exhaust reformers by integrating the heat from the exhaust gas downstream of NG marine engine for the production of hydrogen-rich stream. It was also shown that the heat from the reformer and WGS could be recovered to pre-heat the natural gas and water for steam generation [27]. These studies demonstrated the feasibility of heat integration to reduce the energy intensity of hydrogen production and carbon capture. However, among the choices of hydrogen production methods and carbon capture technologies, which pathway performs the best? Which combination of technologies can give the best performance when being used onboard, given the particular nature of a typical ship engine? A ship-based assessment on various hydrogen production and carbon capture pathways is essential in order to bridge the existing research gap in ship-based hydrogen production.

The novelty of this study is an analysis of the concept of onboard decarbonization with pre-combustion carbon capture and with a special focus on heat integration and optimization. In the next section, the research flow and details of process simulation are presented. Section 3 includes a comparison of the alternative H₂ production systems, the alternative CCS systems, and an optimized system based on SMR-PSA. Section 4 discusses the results in view of their potential for development into a realistic onboard marine system. Section 5 summarizes the most important conclusions.

2 Methods

2.1 Summary of the Calculations

Previous work [4, 5] suggested hydrogen and onboard CCS installation as potential approaches for shipping decarbonization. Here, the combination of onboard hydrogen production and CCS is investigated in more detail. Due to the difference in the performance of the existing technologies for hydrogen production, a comparative study between various technologies is necessary, and a quantification on the energy requirement helps to reflect the feasibility of hydrogen production onboard a ship in terms of energy and CO₂ reduction. In this paper, we compare the overall efficiency of (a) the conventional, unabated ship (Fig. 1a); (b) a post-combustion (post-engine)

CCS system based on amine absorption (Fig. 1b); (c) various pre-combustion CCS systems (Fig. 1c), exploring different H_2 production and carbon capture methods; and (d) an optimized, integrated steam reformer/water-gas shift/pressure swing adsorption system using waste heat recovery (Fig. 3, discussed later). These specific options were selected for optimization because, as will be demonstrated later, they offer the smallest energy penalty for capturing carbon. Figure 2 demonstrates schematically the methodology used and the various reactor options studied. More details follow next.

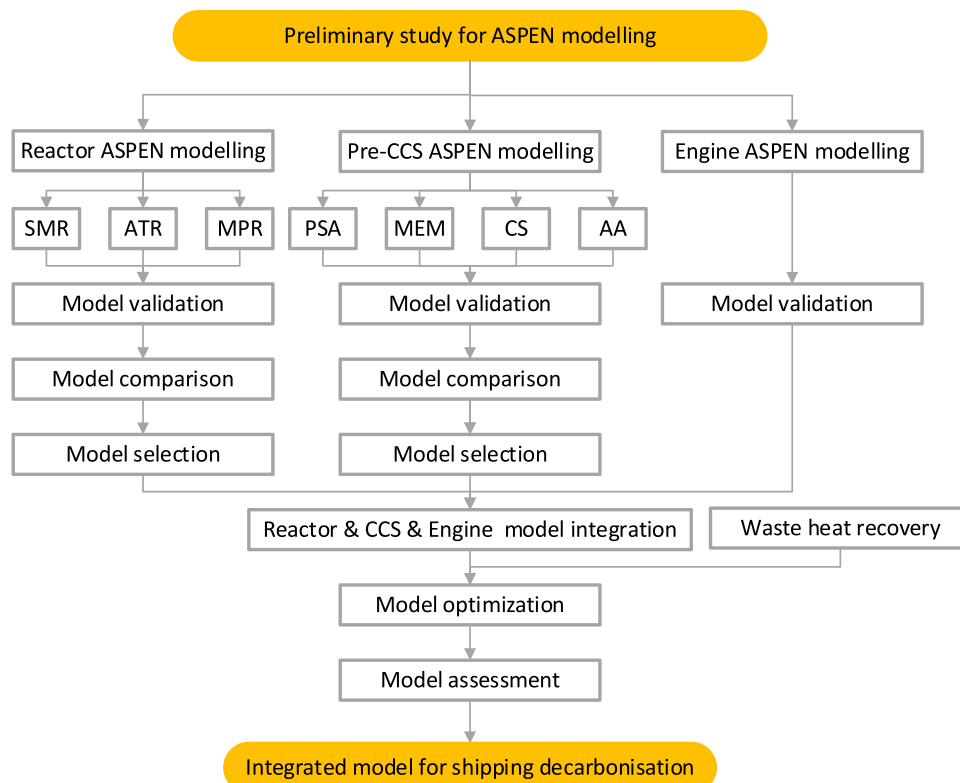
Figure 2 shows schematically the various components of the calculation. Thermodynamics modelling with Aspen HYSYS for different stand-alone hydrogen production and carbon capture systems was first done. Next, the hydrogen production models were optimized for maximum hydrogen production rate. The energy requirements of various reactors for optimal hydrogen production were then reported in terms of kWh/kg CH_4 feed. The mass and energy balance data obtained from the Aspen simulation models were important inputs for energy and GHG assessments so that the energy efficiency (ϵ_0), CO_2 reduction efficiency (β_0), and hydrogen yield (α_{H_2}) could be estimated. These metrics are defined as follows: (a) ϵ_0 is

the measure of the efficiency based on the ratio of engine propulsion work to the overall energy input by the total LNG consumption, (b) β_0 is the ratio of CO_2 captured to the total CO_2 emission if no CCS were installed, and (c) α_{H_2} is the ratio of the hydrogen produced to the maximum possible theoretical production of hydrogen if 100% of the methane feed were converted.

Next, the validated CCS Aspen HYSYS models that were built according to the current state of the art of carbon capture technologies were connected with the product stream from the selected reactor, and hence, the energy requirement of different CCS technologies was obtained in units of kWh/kg CO_2 captured. From these results, a suitable reactor-CCS-integrated system was selected.

The selected reactor-PreCCS-integrated system was combined with the engine model in Aspen HYSYS. With this, an integrated Aspen model for hydrogen production onboard of ship was produced. The operating conditions of the integrated system were optimized with the integration of waste heat. These parameters were (a) the fraction of methane feed that is fed to the SMR furnace (X_{CH_4}) for the generation of heat for the reforming reaction; (b) the steam to methane ratio (S/C); and (c) the exit temperature of the SMR reactor (T_{SMR}).

Fig. 2 Research methodology and flow diagram



Finally, the possibility of using this integrated system for partial reforming, so that the engine is burning some LNG directly and some H_2 produced from the reformer, was investigated to examine whether partial decarbonization can be achieved and what would be the associated energy efficiency and carbon emission.

2.2 Process Simulation of the Various Sub-systems

2.2.1 Hydrogen Production

Aspen models for steam reforming (SMR), autothermal reforming (ATR), and methane pyrolysis (MPR) were constructed. The hydrogen production from liquid methane feedstock via steam reforming and autothermal reactions was modelled as Gibbs reactors, whereby the thermodynamics of the reactions under different operating temperatures and pressures were predicted by using Gibbs free energy minimization method with the Peng-Robinson property package. MPR was modelled as a plug flow reactor using chemical reactions and kinetic parameters taken from Ref. [28]. In the SMR and MPR, some methane needs to be combusted to provide heat for the endothermic reactions. Therefore, the CH_4 processing was modelled using two separate reactors: one was for methane reforming or decomposition and another was the furnace (heater) for methane combustion to provide the required heat. The CO_2 emitted by this process was considered separately. For SMR and ATR, high-temperature and low-temperature water-gas shift reactors (HTWGS and LTWGS) were modelled as Gibbs reactors downstream of the steam reforming reactor unit so that the CO in the product stream was shifted into more hydrogen and CO_2 .

By using experimental or plant data, the Aspen models for the various types of reactors were validated. The SMR model was validated against the experimental data in [29], the ATR model was validated against the BV model presented by De Groote and Froment in Ref. [30], and the MPR was modelled based on the tubular reactor developed from experimental data as published in [28]. The validated models were then used to simulate the hydrogen production process from the feed as described in Table 1 part A. The operating parameters of the reactors as listed in Table 1 part B were manipulated and optimized by using Aspen for a maximum methane conversion and optimal hydrogen production.

Additional unit operations and energy streams were included. For electricity, the power consumptions for pump ($P_{H_2O,pump}$), methane compression (P_{comp}), and oxygen separation (P_{ASU}) were obtained from the model of pump and compressors. In terms of heat utility requirement, heat input for steam generation ($Q_{h,steam}$) and reactor heat requirement ($Q_{h,SMR}$) and heat provided by combustion of methane (Q_{h,CH_4}) were obtained from the energy streams.

Table 1 (A) Feed conditions into the reactor. (B) The adjustable parameters for SMR, ATR, and MPR reactors

A			
Parameters	Properties		
CH_4 feed flow rate (kg/h)	100		
CH_4 storage conditions	−162 °C, 1 bar		
CH_4 lower heating value (kJ/kg)	50,000		
H_2O (seawater) conditions	25 °C, 1 bar		
Steam conditions	230 °C, 25 bar		
Ambient air conditions	25 °C, 1 bar		
B			
Parameters	SMR	ATR	MPR
Methane as fuel in the furnace, X_{CH_4} (%)	15–40	-	1–20
Steam to methane ratio, S/C ratio	2–5	1–2	-
Reactor temperature, T_R (°C)	800–1200	-	-
Oxygen to methane, O/C ratio	-	0–1	-

2.2.2 Carbon Capture and Storage (CCS)

As CO_2 reduction was the main goal of this study, CCS was integrated with the reactor to produce a low-carbon hydrogen stream as the engine feed. For MPR, solid carbon was separated by using a cyclone separator, no heating or power supply was needed, and this separation process did not reduce the overall efficiency of MPR. The shifted syngas downstream of the WGS reactors for SMR and ATR reactors needed to undergo CO_2 separation. In this study, four types of CCS were investigated. These were pressure swing adsorption (PSA), membrane separation (MEM), cryogenic separation (CS), and amine absorption (AA). A comparison of these four types of CCS was performed.

First, Aspen models for PSA, MEM, CS, and AA were constructed and validated. The AA simulation model was based on the optimized blended amine model presented in Ref. [31]. MEM was modelled as a two-staged membrane with CO_2 -selective membrane as the first stage membrane to separate CO_2 as the permeate, followed by H_2 -selective membrane, a MOFs-polymer mixed matrix membrane characterized by [32] with a high H_2 permeance of $33 \times 10^{-9} \frac{mol}{s.Pa.m^2}$, and H_2/CO_2 selectivity of 53.1. PSA was modelled as a single-stage adsorption tower with activated carbon as the adsorbent due to its high selectivity towards CO_2 . Finally, CS was modelled by distillation columns integrated with propane-ethylene cascade refrigeration cycle as proposed in Ref. [33].

To provide a comparison between the pre-combustion CCS studied here and the post-combustion (post-engine) CCS studied in Refs [4, 34–37], the same CCS models were used for the engine exhaust gases. The differences in feed composition and operating conditions gave rise to the

differences in the energy requirement and carbon capture efficiency of the CCS, which are hence worth quantifying.

The CO₂ processing for onboard storage was also modelled downstream of the CCS. The typical storage condition for transportation of CO₂ in liquid form was applied in this study, which was at a temperature of $-20\text{ }^{\circ}\text{C}$ and at 20 bar [38]. Hence, in the modelling of CO₂ storage system, a compressor was used to compress the captured CO₂ to 20 bar, followed by seawater cooling, and finally, the cold energy from regasification of LNG was used to liquefy the CO₂ at $-20\text{ }^{\circ}\text{C}$.

The energy consumption in the various reactors was grouped into electricity and heat utilities in units of kWh per kg of captured CO₂. The electrical power consumption for the various types of CCS was different: PSA and AA required compression power for the captured CO₂ ($P_{\text{CO}_2,\text{comp}}$); MEM required additional power for recompression of the permeate hydrogen before feeding to the combustion engine ($P_{\text{H}_2,\text{comp}}$); and CS required high compression duty to pressurize the feed to 110 bar ($P_{\text{HP,comp}}$) and for compression of the propane and ethylene refrigerants in the cascade refrigeration cycles ($P_{\text{R,Ethylene}}$ and $P_{\text{R,Propane}}$). Next, in terms of heat utilities, the only CCS that consumed heat was the AA unit for the amine regeneration ($Q_{\text{h,CCS}}$). From the total power ($\sum P$) and total heat ($\sum Q$), the total energy consumption ($\sum E$) for the various CCS options was estimated and divided with the total amount of CO₂ captured so that energy requirement was expressed in terms of total kWh/kgCO₂ captured. With this, the energy intensity of various CCS units was compared and analysed numerically and the most suitable CCS for pre-combustion and post-combustion capture was identified.

2.2.3 Combustion Engine (ICE)

We assume that the ship is powered by an internal combustion engine with 48% of energy conversion efficiency (ϵ_{Engine}), representative of a low-speed large marine engine [39]. A simplified engine model with fixed efficiency of 48% was modelled in Aspen. The engine was modelled as a simplified combustion reactor integrated with air compressor and gas turbine for power generation. The exhaust gas condition was assumed with a constant pressure of 1 bar. By using the same engine in the Aspen model, an engine with the usage of methane, hydrogen, or a mixture of methane and hydrogen as marine fuel was simulated. The combustion of LNG and hydrogen gave different compositions of flue gas. The validated engine model was then used for the study of potential heat recovery from the exhaust which was different from the composition of feed fuels. The exhaust from the engine was set at $T = 706.15\text{ K}$.

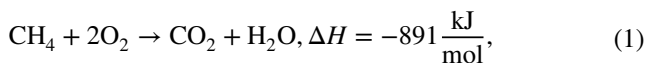
2.2.4 Waste Heat Recovery (WHR)

In the previous steps, the energy requirement of various processes (reactor, CCS) was categorized into heat and electricity requirements. Here, WHR was integrated for the optimization of the SMR-integrated system. As will be shown later, the SMR was the most energy-efficient hydrogen production technology, so this system was selected for optimization and integration. In this study, the heat recoverable was used as heat for steam generation ($Q_{\text{h,steam}}$) and heat for endothermic methane reforming ($Q_{\text{h,SMR}}$). The steam was generated at 503 K, and hence, the exhaust ($T \approx 706\text{ K}$) and product stream from HTWGS ($T > 773\text{ K}$) were used for the steam generation. The product stream from the SMR reactor ($1073\text{ K} < T < 1473\text{ K}$) was used for the pre-heating of methane upstream of the SMR reactor. A temperature below 503 K was assumed as heat loss (Q_{loss}) to the surroundings that could not be further used. The amount of heat recoverable from the exhaust and high-temperature product streams was also estimated using Aspen.

Another potential heat recovery is the heat released from the liquefaction of captured CO₂, which was used for methane gasification. The cryogenic LNG (111.15 K, 1 bar) was vaporized with the heat released from CO₂ liquefaction for storage under 20 bar, 253 K. In this study, seawater was the main cooling medium to cool any streams to 303 K or higher as per process requirement; hence, there was a continuous supply of cooling utilities for ship.

2.2.5 Integrated System

As shown in Fig. 3, the SMR-based integrated system combined the SMR-WGS reactors, PSA, combustion engine, and the storage system for the captured CO₂. The high-temperature stream from the SMR product was used for pre-heating the methane feed so that the heat requirement for reforming ($Q_{\text{h,SMR}}$) could be reduced. In Aspen, the heat recoverable from the SMR product was modelled as an energy stream $Q_{\text{WHR,SMR}}$. The total required heat $Q_{\text{h,SMR}}$ was higher than the $Q_{\text{WHR,SMR}}$; hence, extra heat was supplied by direct combustion of some methane in the SMR furnace. The fraction of the total methane flow to be combusted as fuel (X_{CH_4}) was calculated by using Eqs. (1), (2), and (3), and the heat provided from combustion of methane is represented by $Q_{\text{h,CH}_4}$.



$$Q_{\text{h,CH}_4} = Q_{\text{h,SMR}} - Q_{\text{WHR,SMR}}, \quad (2)$$

$$X_{\text{CH}_4}(\%) = \frac{Q_{\text{h,CH}_4}(\text{kJ})}{\text{LNG feed}(\text{kg})} \times \frac{\text{kmol}}{891,000\text{ kJ}} \times \frac{16.05\text{ kg}}{\text{kmol}} \times 100\%. \quad (3)$$

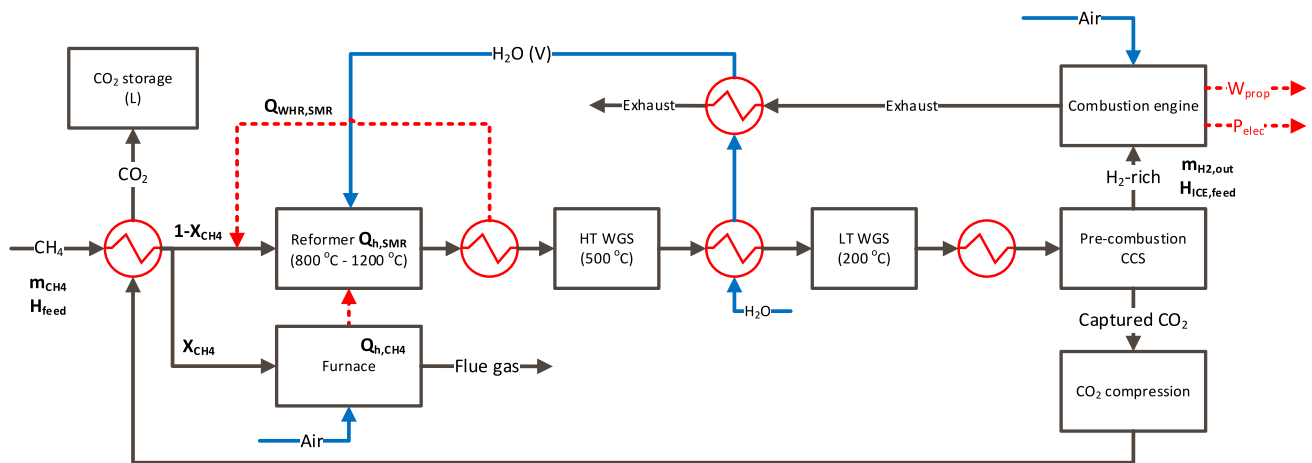


Fig. 3 Block diagram of the SMR-WGS system with pre-combustion CCS describing the processes involved in hydrogen production, hydrogen purification, carbon capture and storage, and combustion engine. The locations of heat exchange between process streams are also indicated

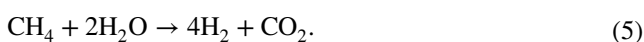
Next, the high-temperature streams from the HTWGS reactor and exhaust were used for steam generation. These streams were inter-connected into a heat exchanger so that the heat could be transferred to heat up and vaporize the cold water feed. The steam was then connected to the reformer for steam methane reforming reaction, while unused steam in the synthesis gas was sent to the HTWGS and LTWGS so that the CO product could be shifted to produce more hydrogen. Next, the shifted syngas produced by the LTWGS was fed into the CCS for the separation of CO₂. The captured CO₂ was compressed and cooled by utilizing the cold energy from the LNG which was stored under cryogenic condition. In Aspen, the heat transfer between the cold LNG and CO₂ was modelled as a heat exchanger. The hydrogen-rich stream separated from the CO₂ was fed into the combustion engine for the generation of propulsion energy. Combustion of the hydrogen-rich stream produced a high-temperature exhaust stream, which was one of the high-temperature streams used for steam production.

2.3 Metrics for Assessment

2.3.1 Hydrogen Yield (α_{H_2})

Mass balance data was obtained from the Aspen simulation; for example, the product from the reactor as tabulated in Table 3 part A was important for the determination of the hydrogen production yield as defined by Eq. (4). The maximum theoretical mass flow of hydrogen from the reactor was estimated as per the stoichiometric Eq. (5).

$$\text{Hydrogen yield, } \alpha_{H_2} = \frac{m_{H_2, \text{out}}(\text{theoretical}) - m_{H_2, \text{out}}}{m_{H_2, \text{out}}(\text{theoretical})}, \quad (4)$$



2.3.2 Energy Efficiency (ϵ)

The energy efficiency of the base case was 48%, i.e. a propulsion output of 6.67 kWh/kgCH₄ was the reference of comparison. Firstly, the electricity and energy requirements of various processes were acquired from Aspen. The electricity needs were assumed to be generated by methane also at the same conversion efficiency of 48%. The heat utilities were supplied from the direct combustion of methane fuel. The summation of total electricity ($\sum P$) requirement and total heat ($\sum Q$) requirement gave the total energy ($\sum E$) which came from LNG consumption as per Eq. (6).

Due to the variation in the hydrogen production rate for the different reactors and CO₂ capture rate in the CCS, all the energy consumptions ($\sum P$, $\sum Q$, and $\sum E$) were expressed in terms of kW/kg CH₄ feed to allow a direct comparison. For the hydrogen production system, the efficiency of the reactors was estimated with Eq. (7). Then, for the other systems, overall efficiency was used as an indicator of system efficiency. Part of the engine output was supplied to the electricity consumers in the integrated system: methane compressor, water pump, and CO₂ compressor. The total electricity consumption was indicated as P_{elec} . The total propulsion output (W_{prop}) of the ship was calculated from Eq. (8), whereby the enthalpy of the engine feed ($H_{\text{ICE, feed}}$) was multiplied with 48% (the assumed engine efficiency, ϵ_{Engine}) and with the deduction of P_{elec} . Next, overall efficiency (ϵ_o) was estimated by dividing with the enthalpy of methane feed as per Eq. (9).

$$\text{Total energy, } \sum E = \frac{\sum P}{0.48} + \sum Q, \quad (6)$$

$$\text{Reactor efficiency, } \epsilon_r (\%) = \frac{(H_{\text{feed}} - \sum E)}{H_{\text{feed}}} \times 100\%, \quad (7)$$

$$\text{Propulsion output, } W_{\text{prop}} \text{ (kWh)} = (H_{\text{ICE,feed}} \times \varepsilon_{\text{Engine}}) - P_{\text{elec}}, \quad (8)$$

$$\text{Overall efficiency, } \varepsilon_o \text{ (\%)} = \frac{W_{\text{prop}}}{H_{\text{feed}}} \times 100\%. \quad (9)$$

2.3.3 Carbon Capture Rate

The carbon capture rate is an important indicator of the system's performance. The CO₂ capture rate of the integrated system was calculated by using Eq. (10), whereby the total amount of captured CO₂ was divided by the total CO₂ emission for the base case. Theoretically, the CO₂ emission from the base case without CCS was estimated to be equal to 274 kg/h of CO₂ for 100 kg/h of methane feed, or 2.74 kgCO₂/kg CH₄.

$$\text{CO}_2 \text{ capture rate, } \beta_o \text{ (\%)} = \frac{\text{CO}_{2,\text{st}}}{\text{CO}_{2,\text{base}}} \times 100\%. \quad (10)$$

2.3.4 Analysis of Variance (ANOVA) of the Optimized Integrated System

The integrated system with WHR had increased complexity. The overall energy efficiency of the integrated system was improved with waste heat recovery from high-temperature streams (i.e. the product streams from the reactors and the engine exhaust). These heats were inter-connected within the Aspen model, so an Aspen nested case study was carried out to simulate the variation of operational parameters, X_{CH_4} , S/C , and T_{SMR} , towards the response of the integrated system (ε_o , β_o , and α_{H_2}). The nested case study was done following the stated range and step sizes for various parameters as shown in Table 2. There were 378 simulation runs in total.

Next, the result obtained from Aspen was analysed with ANOVA, so that the interactions between the three operational parameters and the performance indicators (ε_o , β_o , and α_{H_2}) could be estimated quantitatively. Then, optimization was performed by using the ANOVA model, so that the operating conditions for optimal ε_o and β_o can be identified.

2.3.5 Partial Decarbonization Trajectories

The possibility that not all the engine feed was reformed was also explored by considering the case where some LNG went

through the reformer and CCS, while some LNG was combusted directly in the engine without CCS. This would allow a partial decarbonization strategy that can evolve with time to meet the IMO 2030 and 2050 targets. The percentage of total LNG fed for reforming (to provide both the heat needed for the reforming and the CH₄ to be reformed) was denoted by $X_{\text{f,SMR}}$, and the overall efficiency and CO₂ removal were calculated as a function of this fraction.

2.3.6 Economic of Hydrogen Production

In this study, the hydrogen-rich product was produced onboard of a ship via LNG reforming. The economics of the ship-based produced hydrogen was compared with the market price of hydrogen. Here, the operating cost of the reformer-integrated system was estimated with the aid of Aspen Process Economic Analyser (APEA), and then annualized capital cost (ACAPEX) was estimated based on H2A-Lite Model [40] as per land-based hydrogen production system with pre-combustion CCS. The CAPEX cost of equipment was determined for a ship with a rated power of 15,310 kW and an operational life of 20 years. By doing so, the total production cost of hydrogen onboard of ship (C_T) was estimated from Eq. (11) and expressed in the unit of \$/kgH₂ produced. ACAPEX and total OPEX per annum (kWh/year) were summed and divided by the total amount of hydrogen produced per annum so that the total production cost per kg of hydrogen produced could be calculated. From the literature, the cost of blue hydrogen could range from \$1.5 to \$4 depending on the methane cost, whereas the cost of green hydrogen costs between \$2.5 and \$6 [41]. With this, the economics of onboard fuel production could be assessed.

$$\begin{aligned} \text{Total hydrogen production cost, } C_{\text{total}} \text{ (\$/kgH}_2\text{)} \\ = \frac{\text{ACAPEX} + \text{OPEX}}{m_{\text{H}_2}}. \end{aligned} \quad (11)$$

3 Results

3.1 Selection of Hydrogen Production System

Table 3 part A shows the composition of the product stream from SMR, ATR, and MPR per kg of CH₄ feed. Table 3 part B shows the equivalent energy consumptions. SMR (71.53%) was the most efficient method of hydrogen production, followed by MPR (52.04%) and finally ATR (51.66%), which was in agreement with the overall efficiency reported in the literature [16, 17]. ATR showed the lowest overall efficiency due to the highly energy-intensive ASU unit that consumes high power for oxygen separation. As shown in

Table 2 Aspen nested case study simulation set-up

PreCCS	Range	Step size	Total steps
X_{CH_4} (%)	5–30	5	6
S/C	2–5	0.5	7
T_{SMR} (K)	1073–1473	50	9

Table 3 (A) Mass balance of SMR, ATR, and MPR. (B) Energy balance of SMR, ATR, and MPR

A			
Criteria	SMR	ATR	MPR
Optimized operating parameters	$S/C = 2.5$ $O/C = -$ $X_{CH_4} = 29.0\%$	$S/C = 1.5$ $O/C = 0.64$ $X_{CH_4} = -$	$S/C = -$ $O/C = -$ $X_{CH_4} = 7.5\%$
Operating pressure (bar)	25	25	30
Reactor product enthalpy, $H_{ICE,feed}$ (kWh/kgCH ₄)	11.86	11.38	7.80
H ₂ produced (kg/kgCH ₄)	0.3341	0.3302	0.2304
CO ₂ produced (kg/kgCH ₄)	1.6906	2.5933	-
Unreacted CH ₄ (kg/kgCH ₄)	0.0294	0.0130	0.0084
C produced (kg/kgCH ₄)	-	-	0.6862
B			
Energy components	SMR	ATR	MPR
Heat utilities, ΣQ (kWh/kgCH ₄)	1.54	1.30	-
Electricity, ΣP (kWh/kgCH ₄)	0.18	1.38	0.27
Energy requirement, ΣE (kWh/kgCH ₄)	1.92	4.17	0.56
Rated power, P_{prop} (kWh/kgCH ₄)	4.77	3.45	3.47
Reactor energy efficiency, ϵ_R (%)	71.53	51.66	52.04
Overall energy efficiency, ϵ_O (%)	34.34	24.80	24.98

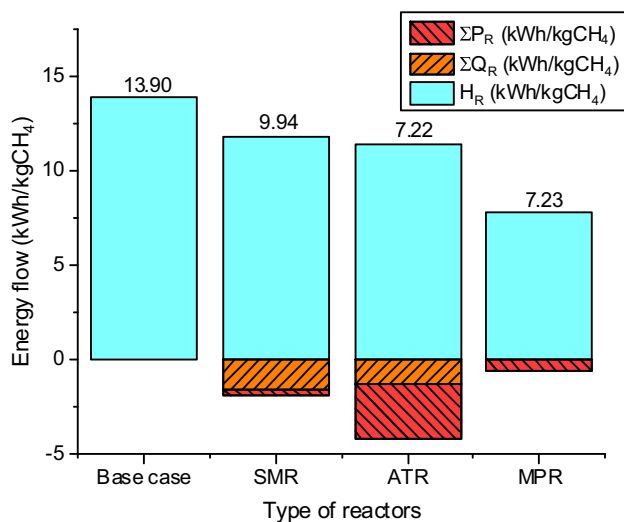
**Fig. 4** Product enthalpy (H_R), total power requirement (ΣP_R), and total energy requirement (ΣQ_R) for the various hydrogen production reactors per kg CH₄ consumed from the LNG feed

Table 3 part B and Fig. 4, the power consumption of ATR was more than seven times the SMR power consumption. This explains the low energy efficiency of ATR and suggests that ATR may not be suitable for ship-based hydrogen production as power utilities were limited for ship. The efficiency of MPR was estimated to be 19.5% lower than SMR, attributed to the energy loss in the form of carbon by-product. MPR combusted 7.5% of the CH₄ feed for heat generation, and approximately 45% of the product's enthalpy from the MPR reactor was lost as carbon product. Due to the

Table 4 (A) Energy balance of PSA, MEM, CS, and AA as pre-combustion CCS (PreCCS). (B) Energy balance of PSA, MEM, CS, and AA as post-combustion CCS (PostCCS)

A				
PreCCS	PSA	MEM	CS	AA
Operating pressure, P (bar)	25	25	110	25
CO ₂ capture rate (%)	$\approx 90\%$	$\approx 81\%$	$\approx 95\%$	$\approx 90\%$
Heat utilities, Q (kWh/kgCO ₂)	-	-	-	1.05
Electricity, P (kWh/kgCO ₂)	0.08	0.28	0.67	0.04
Energy requirement, ΣE (kWh/kgCO ₂)	0.18	0.59	1.40	1.14
B				
PostCCS	PSA	MEM	CS	AA
Operating pressure (bar)	25	25	110	1
CO ₂ capture rate (%)	$\approx 90\%$	$\approx 67\%$	$\approx 90\%$	$\approx 90\%$
Heat utilities, ΣQ (kWh/kgCO ₂)	-	-	-	1.22
Electricity, ΣP (kWh/kgCO ₂)	1.10	1.83	1.43	0.05
Energy requirement, ΣE (kWh/kgCO ₂)	2.29	3.81	2.99	1.33

energy advantage of the SMR, this was selected for further studies of onboard hydrogen generation.

3.2 Comparative Study of Pre-combustion CCS and Post-combustion CCS

Table 4 parts A and B show the energy requirement of PSA, MEM, CS, and AA per 1 kg of captured CO₂ so that the energy of carbon capture can be compared fairly. From Table 4 part A, the PSA was the least energy-intensive

pre-combustion CCS. It consumed 0.18 kWh per kg of captured CO_2 , followed by membrane separation (0.59 kWh/kg CO_2), amine absorption (1.14 kWh/kg CO_2), and lastly cryogenic separation (1.40 kWh/kg CO_2). The PreCCS feed was the gas from the SMR-WGS at high pressure (25 bar), which provided a favourable condition for the CO_2 separation via a different process. Under high pressure, feed compression duty can be avoided for PSA and membrane separation, and the compression duty for the cryogenic separation was also reduced. High pressure also reduced the amount of amine solvent requirement with an increased absorption efficiency. Therefore, the regeneration duty for pre-combustion amine absorption was lower than PostCCS, which occurred at low pressure. In addition, the CO_2 compression duty for CO_2 was also largely reduced. Among all post-combustion capture systems, amine absorption was the least energy intensive with a consumption of 1.33 kWh/kg CO_2 , followed by PSA (2.29 kWh/kg CO_2), cryogenic separation (2.99 kWh/kg CO_2), and membrane separation (3.81 kWh/kg CO_2), as shown in Table 4 part B.

The total energy required to capture 1 kg of CO_2 via PreCCS was approximately 8%, 15%, 47%, and 86% of the total energy required by the PostCCS when PSA, membrane, cryogenic separation, and amine absorption were used respectively. Hence, by comparing the total energy requirement for PreCCS and PostCCS, PreCCS seems to be more energy efficient than post-combustion, with PSA being the least energy-consuming option.

3.3 Selection of Integrated Hydrogen Production-CCS System

Table 5 and Fig. 5 give the results for the SMR-CCS-integrated system. SMR without CCS gave an overall efficiency of 34.34%, and integration of CCS reduced the energy efficiency further. SMR-PSA (33.42%) was the most efficient integrated system, followed by SMR-MEM (31.55%), SMR-AA (28.36%), and lastly SMR-CS (26.53%). This is due to the energy consumption by the CCS which was lowest for PSA, followed by MEM, AA, and CS. Hence, SMR-PSA was the most energy-efficient integrated system.

However, a comparison between SMR and the best pre-combustion CCS and the base case of LNG fuel in the engine with AA post-combustion installation shows that LNG-AA installation was less energy intensive, with 36.62% energy efficiency (see Table 5 part B) as compared to the 33.42% efficiency of SMR-PSA. This can be explained by the highly energy-intensive steam reforming reaction. Hence, post-combustion CCS installation was a more energy-efficient carbon reduction approach for ship, based solely on the outcome of the energy requirements of the reactors. However, the significant heat requirement for the SMR-WGS system

Table 5 (A) Energy balance of SMR-WGS-CCS-integrated system (PreCCS). (B) Energy balance of post-combustion CCS (PostCCS)

A				
PreCCS	SMR-PSA	SMR-MEM	SMR-CS	SMR-AA
$H_{\text{ICE,feed}}$ (kWh/kg CH_4)	11.86	11.86	11.86	11.86
Q_R (kWh/kg CH_4)	1.54	1.54	1.54	3.14
P_R (kWh/kg CH_4)	0.18	0.18	0.18	0.18
Q_{CCS} (kWh/kg CH_4)	0.00	0.00	0.00	1.60
P_{CCS} (kWh/kg CH_4)	0.13	0.39	1.09	0.06
ΣE (kWh/kg CH_4)	2.18	2.72	4.18	3.65
Energy efficiency (%)	33.42	31.55	26.53	28.36
B				
PostCCS	LNG-PSA	LNG-MEM	LNG-CS	LNG-AA
$H_{\text{ICE,feed}}$ (kWh/kg CH_4)	13.90	13.90	13.90	13.90
Q_{CCS} (kWh/kg CH_4)	-	-	-	3.02
P_{CCS} (kWh/kg CH_4)	2.71	3.36	3.54	0.13
ΣE (kWh/kg CH_4)	5.64	7.00	7.38	3.29
Energy efficiency (%)	28.51	23.84	22.51	36.62

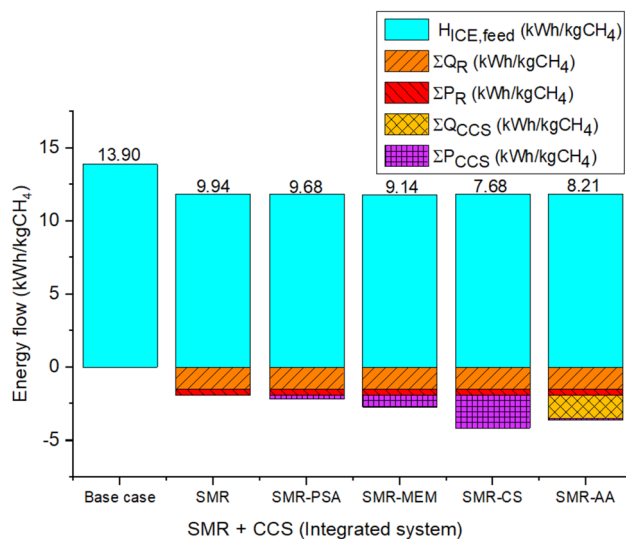


Fig. 5 Product or engine feed enthalpy ($H_{\text{ICE,feed}}$), total power requirement of the reactor and CCS (ΣP_R and ΣP_{CCS}), and total heat requirement of the reactor and CCS (ΣQ_R and ΣQ_{CCS}) of reactor-CCS-integrated system. Results without waste heat recovery.

allows the possibility of effective waste heat utilization, and this is discussed in the next sub-section.

3.4 Optimization of Integrated SMR-PSA with Waste Heat Recovery (WHR)

Figure 6 shows the results of the optimization process, i.e. the selection of X_{CH_4} , S/C , and T_{SMR} so as to maximize overall efficiency. Considering energy optimization, it was found that the lowest X_{CH_4} , S/C , and T_{SMR} gave the highest efficiency. Figure 6 indicates the point with the highest ϵ_o reaches 43.2%, which occurred when $X_{\text{CH}_4} = 15\%$, $S/C = 2$, and $T_{\text{SMR}} = 800$ °C. At this operating condition, the β_o was very low at 41.4%. The optimization of β_o showed that the highest β_o was achieved at a high X_{CH_4} (25%) so that the energy recovered was fully utilized and the additional energy requirement was supplied via combustion of extra methane feed. The point with the highest β_o (66.3%) gave a relatively low energy efficiency of 40.9%. From this, we can conclude that there is a trade-off between ϵ_o and β_o . Finally, examination of the integrated system for optimal ϵ_o and β_o suggested to trade off the highest ϵ_o and β_o with optimal ϵ_o and β_o . The box in Fig. 6 indicates the zone with optimal ϵ_o and β_o , with ϵ_o ranging between 40 and 42% and β_o ranging between 58 and 63%.

ANOVA optimization suggested the operational parameters X_{CH_4} , S/C , and T_{SMR} to be set at 23.68%, 3.163, and 1072 °C. At these conditions, the ϵ_o and β_o increased to


41.7% and 64.9% respectively. ϵ_o increased by 24.78% with WHR, whereas the β_o also increased from 55.53 to 64.9%, showing a 16.87% increment. Hence, WHR was proven to be highly effective in reducing the energy requirement and increasing carbon reduction. The WHR reduced the amount of X_{CH_4} requirement when some of the heat can be recovered from other processes so that more methane can be fed into SMR for reforming. This resulted in a higher α_{H_2} . At the same time, the enthalpy of the SMR product or engine feed ($H_{\text{ICE,feed}}$) was higher and ϵ_o was improved. Also, more CO_2 was captured by the PSA, which improved the β_o of the integrated system.

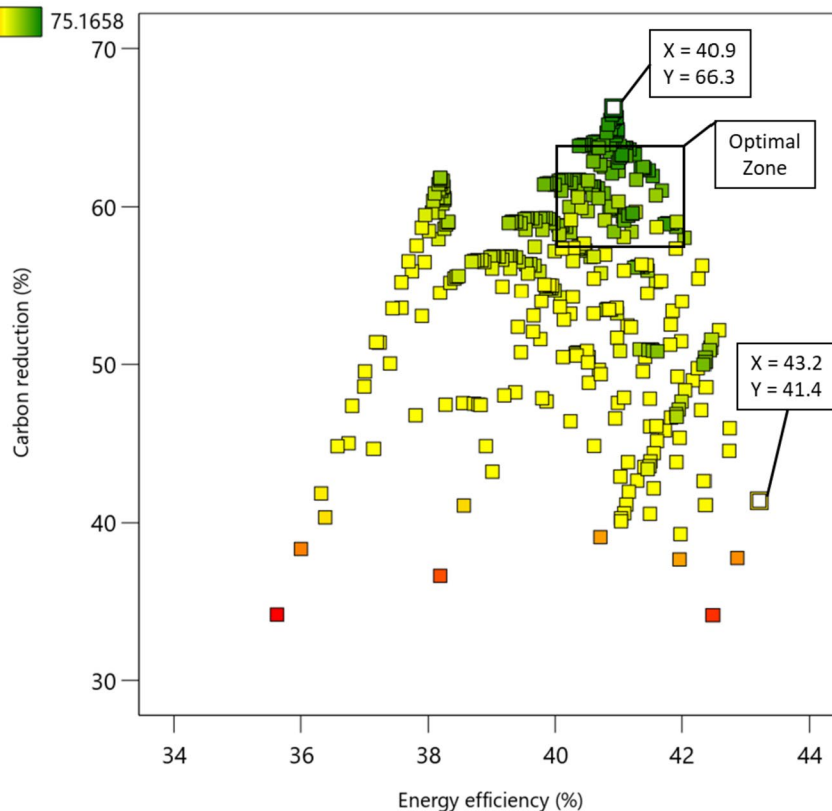
In short, the energy efficiency of the optimal SMR-PSA with WHR (41.70%) was higher than the base case ship with amine-based post-combustion CCS, LNG-AA (36.62%). This suggests that the SMR-integrated system with WHR can have a high energy efficiency and good carbon removal rate. A proper design of the waste heat networks is therefore vital for the improvement of the overall energy efficiency.

3.5 Integrated System in Partial Decarbonization Trajectory

It is instructive to also consider partial decarbonization so that the engine is fed by a mixture of LNG and a reformat.

Fig. 6 Plot of CO_2 reduction rate (β_o) against energy efficiency (ϵ_o) based on the 378 Aspen runs, coloured according to the hydrogen yield. The points with highest ϵ_o , highest β_o , and the region of optimal ϵ_o and β_o are highlighted

Color points by
Hydrogen production rate
39.103  75.1658



A simplified block diagram of this dual-fuel system is shown in Fig. 7. The blocks coloured in blue show the reformer-PreCC system.

Figure 8 shows this scenario in terms of overall efficiency and carbon removal rate as a function of the fraction of CH₄ that is fed to the reformer system (and hence CCS). Hence, X_{f,SMR} = 0% is today’s situation where the engine uses 100% LNG, while X_{f,SMR} = 100% is when the engine used only

the reformat gas. It is evident that by increasing X_{f,SMR}, the degree of decarbonization increases. The overall efficiency penalty to achieve 65% carbon removal is about 7 percentage points.

Figure 9 is plotting the same results, but now with the addition of a second CCS unit based on amine absorption to capture the CO₂ emissions from the CH₄ burning for the SMR. Although this could be practically complicated for

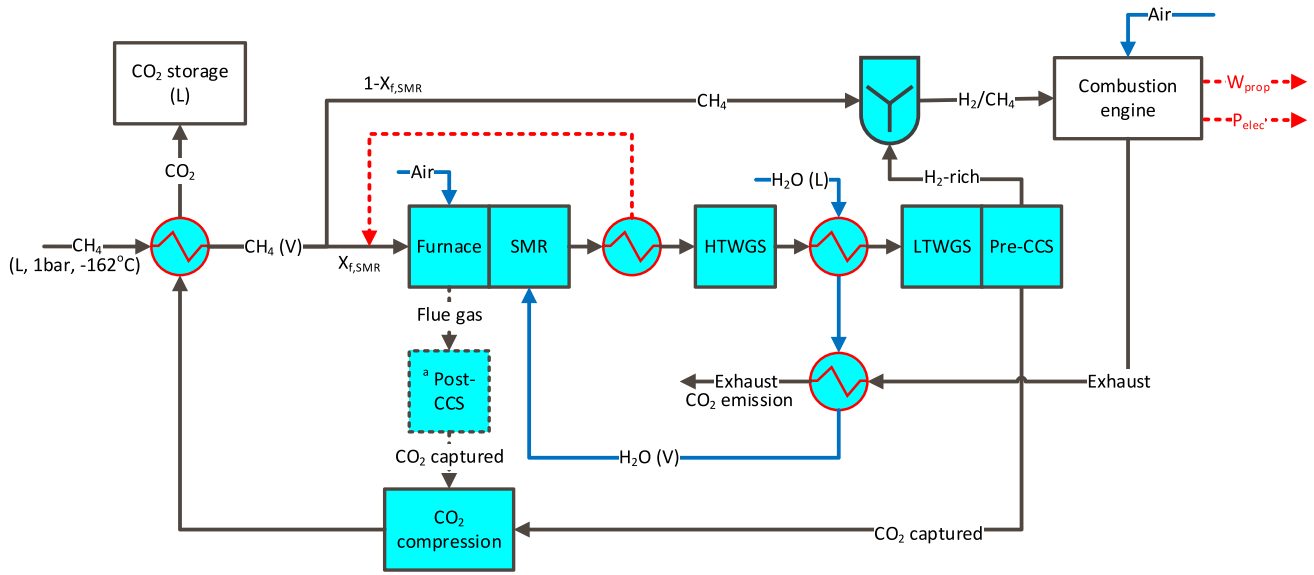
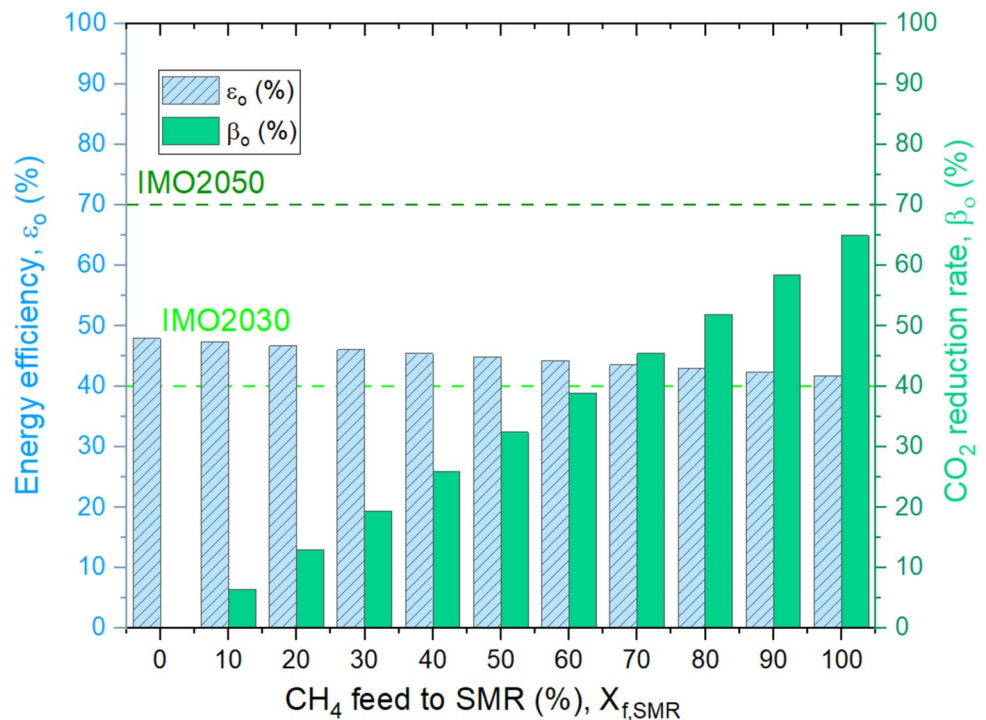


Fig. 7 Block diagram of partial reforming SMR-WGS-CCS-integrated system. Note: The installation of PostCCS for the reformer’s furnace is optional and is included for completeness

Fig. 8 Energy efficiency (ϵ_o) and CO₂ reduction rate (β_o) against the % CH₄ feed into the SMR-integrated system ($X_{f,SMR}$)



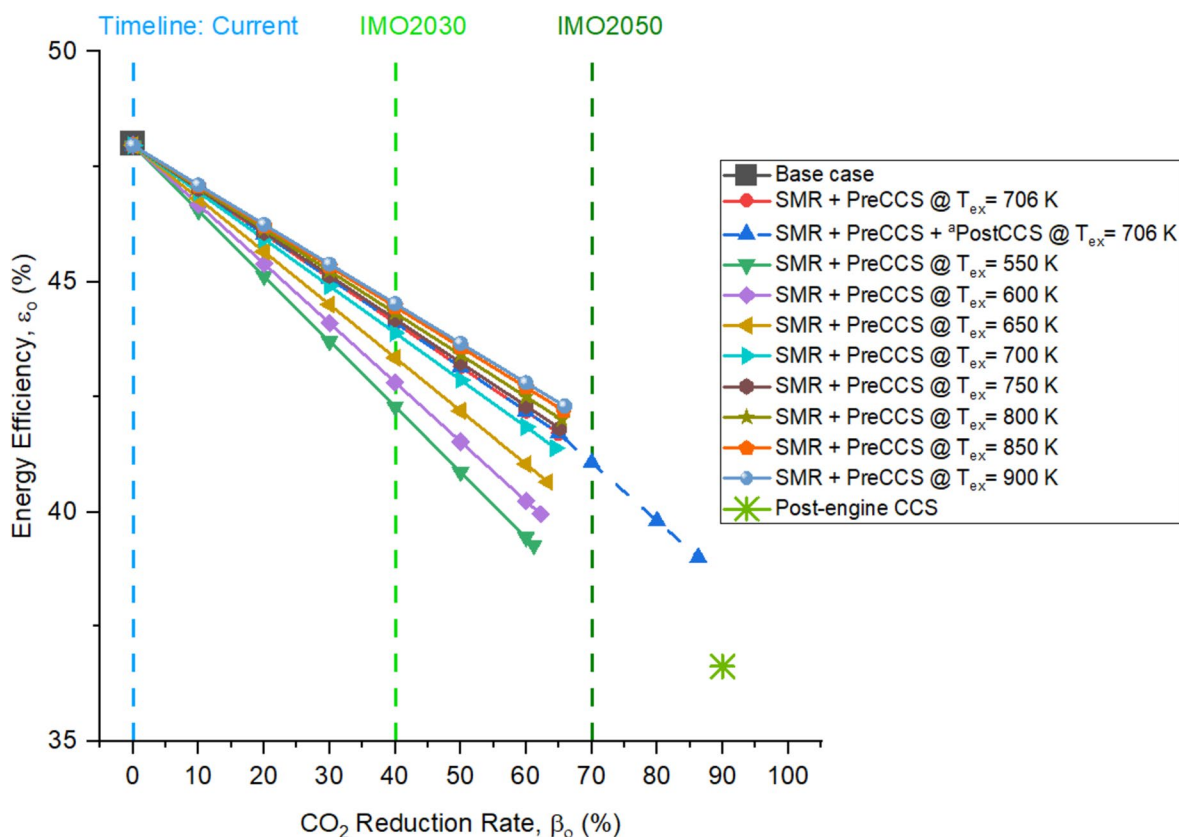


Fig. 9 Overall energy efficiency (ϵ_0) against CO_2 reduction rate (β_0) for the base case (no CCS; squares), reformer-PreCCS system at the design engine exhaust temperature of $T_{\text{ex}} = 433$ K, reformer-PreCCS at various exhaust temperatures ($550 \text{ K} < T_{\text{ex}} < 900 \text{ K}$), and a refer-

ence point of post-engine CCS with $\beta_0 = 90\%$ (star). The blue upright triangles show the case where amine CCS is also included to capture the SMR heater CO_2 emission

implementation, this calculation is included here for completeness. The β_0 is now maximized to 86.3% and the energy efficiency is reduced to 39%. The maximum β_0 of SMR-integrated system is slightly lower than the base case with post-combustion CCS ($\beta_0 = 90\%$). However, the ϵ_0 of the SMR-integrated system ($\epsilon_0 = 39\%$) is about 6% higher than LNG-CCS ($\epsilon_0 = 36.6\%$).

Figure 9 shows the changes in the ϵ_0 and β_0 for the reformer system when the exhaust temperature (T_{ex}) was varied. It was discovered that a higher exhaust temperature improved the ϵ_0 and β_0 for the system. When T_{ex} was low, additional methane was burnt to generate heat for steam generation as the heat recovered from the exhaust stream was insufficient. At a high T_{ex} , more heat can be recovered from the exhaust stream which allows the generation of steam with higher temperature, which indirectly reduces the $Q_{\text{h,SMR}}$ requirement, and hence, a lower $Q_{\text{h,CH}_4}$ is needed for the reformer.

The decarbonization timeline as shown in Fig. 9 shows that both IMO2030 and IMO2050 goals can be met with either an SMR-PSA integrated pre-combustion CCS system or a post-combustion CCS system. However, the

pre-combustion CCS systems exhibit better overall efficiency, suggesting that the proposed system has a promising outlook for shipping decarbonization.

3.6 Economic of Hydrogen Production

The economics of hydrogen production was projected by using the optimal model of SMR-PSA with WHR ($\epsilon_0 = 41.70\%$) discussed in Section 3.4. A ship with a rated power of 15,310 kW and energy efficiency of 41.70% required 63,407 kg CH_4 /day (880,729 kWh/day to produce approximately 26,072 kg H_2 /day). Based on this hydrogen production rate, the total installed CAPEX was estimated using H2A-Lite Model to be \$249,246,259. Assuming that a ship was designed to operate for 20 years, the ACAPEX was \$12,462,313/year or \$1.31/kg H_2 . The OPEX cost was estimated based on the total consumption of methane feedstock, as electricity and heat utilities were both obtained from methane feed for a ship-based operation. For production of 26,072 kg H_2 /day, 63,407 kg CH_4 /day was consumed. Based on the selling price of methane of \$239/tons CH_4 [42], the OPEX cost was calculated to be \$5,531,344/year or

\$0.58/kgH₂. Hence, the total cost of 1 kg of blue hydrogen produced onboard of ship with SMR-PSA is \$1.89.

4 Discussion

This study has introduced a new concept for onboard carbon capture for LNG-fuelled shipping by combining two energy-intensive systems, hydrogen production, and onboard carbon capture, with effective heat integration from the LNG and the engine exhaust. The performance of the proposed system was measured in terms of overall energy efficiency (ϵ_o) and carbon capture fraction (β_o). The combination of SMR and PSA was proposed as SMR was more energy efficient than ATR and MPR (Table 3 and Fig. 4), and as PSA had the lowest energy consumption compared to alternative CCS methods (MEM, AA, and CS; see Table 4). The integrated system SMR-PSA resulted in a significant reduction of overall efficiency from 48 to 33.42% (see Table 5). However, optimization with WHR improved the energy efficiency of the system to achieve $\epsilon_o = 41.7\%$. Therefore, this reformer system was able to reduce 65% of carbon emission with an energy penalty of about 7 percentage points.

Compared to post-engine CCS, which is the usual shipping decarbonization proposition based on CCS, a reformer system produces syngas with a higher concentration of CO₂, which eases the carbon capture process, especially for a ship-based CCS with space constraints. Handling a smaller flow of syngas fuel than the much larger flow of flue gas produced downstream of the engine is highly favourable as this would be able to reduce the CCS size and minimize the ship space for accommodation of the CCS unit. It is also expected to have lower capital cost. In addition, a PSA-based CO₂ capture process can reduce the risk and hazards associated with chemical handling and storage onboard. An additional advantage of the reforming and pre-combustion CCS is that it can also be considered “onboard blue hydrogen production” which eliminates the need to have a separate LH₂ bunkering infrastructure and onboard LH₂ tanks. This implies that the problem of large LH₂ boil-off is eliminated and should result in a lower financial burden. Further, hazards associated with hydrogen handling are probably easier to manage, since the path from production to utilization is much shortened compared to land-based hydrogen production, bunkering, and use on the ship. Therefore, if blue hydrogen production is to happen, the present results suggest it is advantageous to do this onboard rather than on land.

The reformer system being proposed in this study consists of steam methane reformer and PSA. Globally, 95% of the hydrogen is produced from the SMR process. PSA is also a commercialized carbon capture technology with high TRL, widely used by the hydrogen industry players like Honeywell and Linde [43, 44]. So, the proposed system, which is an

integration of two matured technologies, should be possible to achieve. From an economic perspective, the cost of 1 kg of blue hydrogen produced onboard of ship with SMR-PSA was estimated to be \$1.89. As compared to the current price of blue hydrogen fuel which ranges from \$1.5 to \$4/kg [45], in situ production of hydrogen from methane is within the range of the average market price of hydrogen. In addition, the boil-off rate of hydrogen is almost 9 times higher than LNG ship [11], and then as much as 45% of the purchased liquefied hydrogen was reported to loss during fuel transportation and bunkering [46]. With such high amounts of fuel loss, the OPEX cost of ship powered by purchased hydrogen could be higher. Thus, production of blue hydrogen onboard the ship offers a reasonably cost-effective low-carbon propulsion. However, the sub-systems have not been demonstrated onboard and so their development for a marine environment needs concerted effort. In addition, the good efficiency of the proposed system relies on an effective waste heat recovery system, which implies that retrofitting and redesigning ships need careful multi-partner collaborations including the manufacturer of the propulsion unit so that excessive back pressure is not imposed on it.

Concerning the advantages of this concept for meeting the IMO targets, the following comments can be made. The simplicity, flexibility, and scalability of the concept offer some advantages. The simplicity of PSA operation is an advantage of the proposed system. In terms of flexibility, the SMR-PSA concept is suitable for ships fitted with dual-fuel engines, irrespective of whether these are 2- or 4-stroke. One may also consider starting with a smaller degree of decarbonization in the beginning and reform and capture a higher percentage as time evolves. At this moment when the carbon taxes are much lower than the estimated CAPEX and OPEX of most decarbonization technologies, a full-scale investment on decarbonization technologies is an expensive solution. The system can be upscaled to meet the reduction targets from time to time. Moreover, the replacement of traditional diesel generators with fuel cells can also be considered for further improvement on ship energy and reduction efficiencies. However, the reformat may need further purification depending on the type of fuel cell employed. Finally, we should mention that the current proposal offers flexibility for future propulsion systems, e.g. based on hybrid modes, gas turbines, or fuel cells. Each of these applications would need optimization of the integrated reformer-CCS-combustion system following the methodology presented in this paper and an increase in TRL by pilot and demonstration projects before commercial deployment.

5 Conclusions

In this paper, an integrated reformer system with waste heat recovery was assessed thermodynamically. A comparison of SMR, ATR, and MPR hydrogen production units showed

that SMR is the most energy-efficient hydrogen production system ($\epsilon_r = 71.5\%$), approximately 20% more energy efficient than ATR and MPR. SMR also has the highest hydrogen production rate, about 2% and 31% higher than ATR and MPR respectively. A comparison of CCS options (Table 4 part A) showed that PSA consumed 2.3 times, 5.3 times, and 6.8 times less energy than MEM, AA, and CS respectively in pre-combustion capture per unit mass of CO_2 . Hence, the SMR-PSA system was selected for further analysis. Optimization of the integrated system suggested to operate the reformer at 23.68%, 3.163, and 1072 °C for the operational parameters X_{CH_4} , S/C , and T_{SMR} respectively. This operation yielded an optimal ϵ_o and β_o of 41.7% and 64.9% respectively. From Fig. 8, it was also shown that a higher CO_2 reduction rate was traded off with lower energy efficiency. This system was able to meet the IMO2030 CO_2 reduction target ($\beta_o = 40\%$) with mixed fuel of 62% CH_4 fed into the SMR-WGS-CCS-integrated system ($X_{\text{f,SMR}}$) and the remaining 38% of methane directly fed into the combustion engine. Full reforming reached 65% CO_2 capture at an overall efficiency of 41%. This is not far from IMO2050, considering that the baseline for the IMO reduction is 2008 emissions with HFO operation. The efficiency penalty of the pre-combustion CCS/LNG reformer depends on the engine exhaust temperature (Fig. 9), implying that in practice the combination reformer/CCS/engine must be optimized together. The present results suggest that producing hydrogen onboard the ship and capturing the CO_2 at the reformer stage offer an attractive marine decarbonization strategy.

Author contributions L.C.L., E.M., and A.T. were involved in conceptualization; L.C.L. and E.M. wrote the main manuscript and analysed the results; L.C.L. prepared all the tables and figures; and E.M., M.R.O., and A.T. reviewed and edited the article.

Funding This research was funded by the National Research Foundation (NRF), Prime Minister's Office, Singapore, under its Campus for Research Excellence and Technological Enterprise (CREATE) programme.

Compliance with ethical standards

The authors declare that they have no competing interests.

Open Access This article is licensed under a Creative Commons Attribution 4.0 International License, which permits use, sharing, adaptation, distribution and reproduction in any medium or format, as long as you give appropriate credit to the original author(s) and the source, provide a link to the Creative Commons licence, and indicate if changes were made. The images or other third party material in this article are included in the article's Creative Commons licence, unless indicated otherwise in a credit line to the material. If material is not included in the article's Creative Commons licence and your intended use is not permitted by statutory regulation or exceeds the permitted use, you will need to obtain permission directly from the copyright holder. To view a copy of this licence, visit <http://creativecommons.org/licenses/by/4.0/>.

References

- Mission Innovation, "Zero-emission shipping," Mission Innovation, 2022. <http://mission-innovation.net/missions/shipping/>. [Accessed 2 December 2022].
- Christos Chryssakis, Pewe, H.: LNG as ship fuel. DNVGL (2021)
- S. U. Khalid, "Safety features on LNG powered ships," Marine Insights, 28 June 2022. . <https://www.marineinsight.com/marine-safety/safety-features-on-lng-ships/>. [Accessed 06 December 2022].
- Law, L.C., Mastorakos, E., Evans, S.: Estimates of the decarbonisation potential of alternative fuels for shipping as a function of vessel type, cargo, and voyage. *Energies*. **15**(7468), (2022). <https://doi.org/10.3390/en15207468>
- Law, L.C., Foscoli, B., Mastorakos, E., Evans, S.: A comparison of alternative fuels for shipping in terms of lifecycle energy and cost. *Energies*. **14**(24), (2021). <https://doi.org/10.3390/en14248502>
- Executive, T.M.: Concept to produce hydrogen on LNG ships to overcome obstacles. The Maritime Executive (2021) <https://www.maritime-executive.com/article/concept-to-produce-hydrogen-on-lng-ships-to-overcome-obstacles>. [Accessed 20 March 2023]
- HyShip, "HyShip," HyShip, 2021. <https://hyship.eu/>. [Accessed 2 December 2022].
- Wilhelmsen, "Wilhelmsen," Wilhelmsen, 17 December 2020.. <https://www.wilhelmsen.com/media-news-and-events/press-releases/2020/wilhelmsens-topeka-hydrogen-project-awarded-nok-219-million/>. [Accessed 2 December 2022].
- A. BIOGRADLIJA, "HySeas III project to build hydrogen-powered ferry," Energy News, 7 June 2021. . <https://energynews.biz/hyseas-iii-project-to-build-hydrogen-powered-ferry/>. [Accessed 15 April 2022].
- Imamura, T., Mogi, T., Wada, Y.: Control of the ignition possibility of hydrogen by electrostatic discharge at a ventilation duct outlet. *Int. J. Hydrog. Energy*. **34**, 2815–2823 (2009). <https://doi.org/10.1016/j.ijhydene.2009.01.028>
- Smith, J.R., Gkantonas, S., Mastorakos, E.: Modelling of boil-off and sloshing relevant to future liquid hydrogen carriers. *Energies*. **15**, (2022). <https://doi.org/10.3390/en15062046>
- IEA: The future of hydrogen seizing today's opportunities- report prepared by the IEA for the G20, Japan. International Energy Agency, US (2019)
- RINA: A scalable and sustainable proposal with hydrogen as fuel to meet IMO2050 targets. RINA <https://www.rina.org/en/media/press/2021/11/25/ship-hydrogen-fuel>. [Accessed 2 December 2022]
- Marine Link: New ship technology will produce hydrogen on board from LNG. Marine Link <https://www.marinelink.com/news/new-ship-technology-produce-hydrogen-501251>. [Accessed 2 December 2022]
- C-ZERO: Technology. C-ZERO (2021) <https://www.czzero.energy/technology>. [Accessed 3 December 2022]
- Kalamaras, C., Efstathiou, A.M.: Hydrogen production technologies: current state and future developmentS. *Conf. Papers Energy*. **2013**, (2013). <https://doi.org/10.1155/2013/690627>
- Steinberg, M.: Fossil fuel decarbonisation technology for mitigating global warming. *Int. J. Hydrog. Energy*. **24**, 771–777 (1999)
- Sánchez-Bastardo, N., Schlögl, R., Ruland, H.: Methane pyrolysis for zero-emission hydrogen production: a potential bridge technology from fossil fuels to a renewable and sustainable hydrogen economy. *Ind. Eng. Chem. Res.* **60**, 11855–11881 (2021). <https://doi.org/10.1021/acs.iecr.1c01679>
- Oni, A., Anaya, K., Giwa, T., Lullo, G.D., Kumar, A.: Comparative assessment of blue hydrogen from steam methane reforming,

- autothermal reforming, and natural gas decomposition technologies for natural gas-producing regions. *Energ. Conver. Manage.* **254**, (2022). <https://doi.org/10.1016/j.enconman.2022.115245>
20. Pashchenko, D.: Performance evaluation of a combined power generation system integrated with thermochemical exhaust heat recuperation based on steam methane reforming. *Int. J. Hydrog. Energy.* **48**(15), 5823–5835 (2022). <https://doi.org/10.1016/j.ijhydene.2022.11.186>
 21. Huang, Y., Zhang, Z., Long, Y., Zhang, Y., Li, G., Zhou, M.: Hydrogen production and energy efficiency optimization of exhaust reformer for marine NG engines: a view of surface reaction kinetics. *Fuel.* **336**, (2023). <https://doi.org/10.1016/j.fuel.2022.127051>
 22. Pruvost, F., Cloete, S., Pozo, C.A.D., Zaabout, A.: Blue, green, and turquoise pathways for minimizing hydrogen production costs from steam methane reforming with CO₂ capture. *Energ. Conver. Manage.* **274**, (2022). <https://doi.org/10.1016/j.enconman.2022.116458>
 23. Pashchenko, D., Mustafin, R., Karpilov, I.: Thermochemical recuperation by steam methane reforming as an efficient alternative to steam injection in the gas turbines. *Energy.* **258**, (2022). <https://doi.org/10.1016/j.energy.2022.124913>
 24. Long, Y., Li, G., Zhang, Z., Wei, W., Liang, J.: Hydrogen-rich gas generation via the exhaust gas-fuel reformer for the marine LNG engine. *Int. J. Hydrog. Energy.* **47**, (2022). <https://doi.org/10.1016/j.ijhydene.2022.02.188>
 25. Yin, Z., Cai, W., Zhang, Z., Deng, Z., Li, Z.: Effects of hydrogen-rich products from methanol steam reforming on the performance enhancement of a medium-speed marine engine. *Energy.* **256**, (2022). <https://doi.org/10.1016/j.energy.2022.124540>
 26. Zhang, Z., Wu, R., Feng, S., Long, Y., Li, G.: Numerical investigation of tubular exhaust reformer with thermochemical recuperation for LNG engine. *Int. J. Heat Mass Transf.* **146**, (2020). <https://doi.org/10.1016/j.ijheatmasstransfer.2019.118743>
 27. Song, C., Liu, Q., Ji, N., Kansha, Y., Tsutsumi, A.: Optimization of steam methane reforming coupled with pressure swing adsorption hydrogen production process by heat integration. *Appl. Energy.* **154**, 392–401 (2015). <https://doi.org/10.1016/j.apenergy.2015.05.038>
 28. Kobayashi, A., Steinberg, M.: The thermal decomposition of Methane in a tubular reactor. Department of Applied Science - Brookhaven National Laboratory, New York (1992)
 29. Ryi, S.-K., Park, J.-S., Kim, D.-K., Kim, T.-H., Kim, S.-H.: Methane steam reforming with a novel catalytic nickel membrane for effective hydrogen production. *J. Membr. Sci.* **339**, 189–194 (2009). <https://doi.org/10.1016/j.memsci.2009.04.047>
 30. Groote, A.M.D., Froment, G.F.: Simulation of the catalytic partial oxidation of methane to synthesis gas. *Appl. Catal. Gen.* **138**, 245–264 (1996)
 31. Law, L.C., Azudin, N.Y., Shukor, S.R.A.: Optimisation of operational parameter and economic analysis of amine based acid gas capture unit. *Chem. Eng. Trans.* **56**, (2017). <https://doi.org/10.3303/CET1756013>
 32. Zhao, Y., Zhao, D., Kong, C., Zhou, F., Jiang, T., Chen, L.: Design of thin and tubular MOFs-polymer mixed matrix membranes for highly selective separation of H₂ and CO₂. *Sep. Purif. Technol.* **220**, 195–205 (2019). <https://doi.org/10.1016/j.seppur.2019.03.037>
 33. Guido, G.D., Lange, S., Pellegrini, L.A.: Refrigeration cycles in low-temperature distillation processes for the purification of natural gas. *J. Nat. Gas Sci. Eng.* **27**, 887–900 (2015). <https://doi.org/10.1016/j.jngse.2015.09.041>
 34. Law, L.C., Othman, M.R., Mastorakos, E.: Numerical analyses on performance of low carbon containership. *Energy Rep.* **9**, 3440–3457 (2023). <https://doi.org/10.1016/j.egy.2023.02.035>
 35. Stec, M., Tatarczuk, A., Iluk, T., Szul, M.: Reducing the energy efficiency design index for ships through a post-combustion carbon capture process. *Int. J. Greenh. Gas Control.* **108**, (2021). <https://doi.org/10.1016/j.ijggc.2021.103333>
 36. Feenstra, M., Monteiro, J., van den Akker, J.T., Abu-Zahra, M.R., Gilling, E., Goetheer, E.: Ship-based carbon capture onboard of diesel or LNG-fuelled ships. *Int. J. Greenh. Gas Control.* **85**, 1–10 (2019)
 37. Ji, C., Yuan, S., Huffman, M., El-Halwaji, M.M., Wang, Q.: Post-combustion carbon capture for tank to propeller via process modeling and simulation. *J. CO₂ Util.* **51**, (2021). <https://doi.org/10.1016/j.jcou.2021.101655>
 38. GreenFacts, "CO₂ capture and storage," GreenFacts, 5 April 2022. <https://www.greenfacts.org/en/co2-capture-storage/l-3/4-transport-carbon-dioxide.htm>. [Accessed 30 January 2023].
 39. Hannu Jääskeläinen, "Natural gas engines," DieselNet, November 2022. https://dieselnet.com/tech/engine_natural-gas.php. [Accessed 31 December 2022].
 40. NREL, "H₂A-Lite: hydrogen analysis lite production model download," <https://www.nrel.gov/hydrogen/h2a-lite-download.html>. [Accessed 21 May 2023].
 41. Global Energy, Global Energy, 1 April 2022. <https://globalenergyprize.org/en/2022/04/01/hydrogen-at-one-dollar-per-kilogram/>. [Accessed 24 May 2023].
 42. Lee, S., Kim, H.S., Park, J., Kang, B.M., Lim, H., Won, W.: Scenario-based techno-economic analysis of steam methane reforming process for hydrogen production. *Appl. Sci.* **11**, (2021). <https://doi.org/10.3390/app11136021>
 43. Honeywell: Honeywell Technology Enables Large U.S. Carbon Capture And Storage Project. Honeywell <https://www.honeywell.com/us/en/press/2021/04/honeywell-technology-enables-large-us-carbon-capture-and-storage-project>. [Accessed 22 March 2023]
 44. Engineering, L.: Adsorption-based carbon capture and CO₂ recovery. Linde Engineering <https://www.linde-engineering.com/en/process-plants/adsorption-and-membrane-plants/adsorption-based-carbon-capture-and-co2-recovery/index.html>. [Accessed 22 March 2023]
 45. N. Simon, McCurdy, P.E. and H. M. Larson, "Examining the current and future economics of hydrogen energy," <https://www.icf.com/insights/energy/economics-hydrogen-energy>. [Accessed 16 July 2023].
 46. Kim, J.H., Park, D.K., Kin, T.J., Seo, J.K.: Thermal-structural characteristics of multi-layer vacuum-insulated pipe for the transfer of cryogenic liquid hydrogen. *Metals.* **12**(4), (2022). <https://doi.org/10.3390/met12040549>

Publisher's Note Springer Nature remains neutral with regard to jurisdictional claims in published maps and institutional affiliations.

Authors and Affiliations

Li Chin Law^{1,2} · Epaminondas Mastorakos^{1,3} · Mohd. Roslee Othman³ · Antonis Trakakis⁴

✉ Li Chin Law
lcl38@cam.ac.uk

✉ Epaminondas Mastorakos
em257@eng.cam.ac.uk

✉ Mohd. Roslee Othman
chroslee@usm.my

² School of Chemical Engineering, Engineering Campus,
Universiti Sains Malaysia, Nibong Tebal, 14300 Penang,
Malaysia

³ Engineering Department, University of Cambridge,
Cambridge CB2 1PZ, UK

⁴ RINA, Piraeus, Greece

¹ Cambridge Centre for Advanced Research and Education
in Singapore (CARES), CREATE Tower, 1 Create Way,
Singapore 1386021, Singapore